Geophysical Research Letters

RESEARCH LETTER
10.1029/2024GL113877

Special Collection:
The U.S. GEOTRACES Pacific Meridional Transect (GP15)

The Influence of Natural, Anthropogenic, and Wildfire Sources on Iron and Zinc Aerosols Delivered to the North Pacific Ocean

Z. B. Bunnell[1], M. Sieber[1], D. S. Hamilton[2], C. M. Marsay[3,4], C. S. Buck[3], W. M. Landing[5], S. G. John[6], and T. M. Conway[1]

[1]College of Marine Sciences, University of South Florida, St Petersburg, FL, USA, [2]Department of Marine, Earth, and Atmospheric Sciences, North Carolina State University, Raleigh, NC, USA, [3]Skidaway Institute of Oceanography, University of Georgia, Savannah, GA, USA, [4]College of Earth, Ocean, and Environment, University of Delaware, Newark, DE, USA, [5]Department of Earth, Ocean, and Atmospheric Science, Florida State University, Saint Petersburg, FL, USA, [6]Department of Earth Sciences, University of California Los Angeles, Los Angeles, CA, USA

Abstract Atmospheric deposition is an important source of iron (Fe) and perhaps zinc (Zn) to the oceans. We present total and water-soluble aerosol Fe and Zn isotopic compositions, size-fractionated aerosol Fe isotopic compositions, and aerosol enrichment factors from the North Pacific GEOTRACES GP15 section (Alaska-Tahiti) during the low dust season. We found distinct bulk aerosol provinces along this latitudinal transect: Asian aerosols (especially crustal dust) dominate at higher latitudes (52–32°N) while North American heavier-than-crustal wildfire aerosols dominate in Equatorial Pacific deployments (20°N to 20°S). Soluble aerosol Fe was isotopically lighter-than-crustal along the full transect, strongly indicative of a pervasive anthropogenic Fe contribution to the Pacific. Comparison to a global aerosol deposition model corroborates that an isotopically heavy endmember is required for wildfire Fe, attributed to pyroconvective entrainment of soil particles. For Zn, the entire GP15 section is dominated by non-crustal anthropogenic sources, reflected by light isotopic compositions (bulk: −0.12 ± 0.08‰ and soluble: −0.17 ± 0.14‰).

Plain Language Summary Along with nutrients such as nitrate and phosphate, trace metals such as iron and zinc, are required by marine microbes to carry out photosynthesis and other metabolic functions. Atmospheric dust, a combination of natural, anthropogenic, and wildfire aerosols, is a key source of trace metals to the surface of the oceans. Here, we present the concentration and isotopic composition of Fe and Zn in atmospheric aerosols collected over the North Pacific Ocean in a transect from Alaska to Tahiti on the GEOTRACES GP15 section cruise (2018). We find Fe in North Pacific aerosols is sourced principally from natural Asian dust with a component from anthropogenic sources. However, Equatorial Pacific aerosols are also influenced by Fe supplied from Californian wildfires, with observations and models supporting a distinct heavy isotopic signature of this Fe source. Water-soluble aerosol Fe as well as bulk and water-soluble aerosol Zn are all indicative of anthropogenic sources of both metals affecting surface waters throughout the section. Comparison with a dust-deposition model allows us to improve model parameterization and refine Fe isotope endmembers.

Key Points:

- Asian Outflow aerosols are sourced from dust and anthropogenic Fe; Equatorial Pacific aerosols also include a wildfire contribution
- Wildfire Fe is characterized with an isotopically heavy endmember due to pyroconvective entrainment of soil
- Bulk and soluble aerosol Zn are isotopically light throughout the transect, indicating pervasive anthropogenic Zn sources

Supporting Information:

Supporting Information may be found in the online version of this article.

Correspondence to:

Z. B. Bunnell and T. M. Conway,
zbunnell@usf.edu;
tmconway@usf.edu

Citation:

Bunnell, Z. B., Sieber, M., Hamilton, D. S., Marsay, C. M., Buck, C. S., Landing, W. M., et al. (2025). The Influence of natural, anthropogenic, and wildfire sources on iron and zinc aerosols delivered to the North Pacific Ocean. *Geophysical Research Letters*, *52*, e2024GL113877. https://doi.org/10.1029/2024GL113877

Received 12 DEC 2024
Accepted 23 DEC 2024
Corrected 4 MAR 2025

This article was corrected on 4 MAR 2025. See the end of the full text for details.

1. Introduction

Trace metals such as iron (Fe) and zinc (Zn) are important marine micronutrients, with Fe limiting growth over much of the surface oceans (Moore et al., 2013; Morel et al., 1994). Atmospheric dust is a key source of Fe (and perhaps Zn) to the oceans, alongside sediments, rivers, and hydrothermal venting (Conway et al., 2024; Tagliabue et al., 2017). Originally, atmospheric aerosol Fe was thought to consist of natural desert dust, but the importance of anthropogenic (industry and fossil fuel combustion), biomass-burning, and wildfire sources to atmospheric Fe aerosols has now been well established (Hamilton et al., 2022, and references therein). For example, Tang et al. (2021) showed that atmospheric transport of Fe from Australian wildfires to the nearby surface ocean stimulated widespread phytoplankton blooms. The presence of anthropogenically derived metals in aerosols has been inferred using elemental enrichment factors (EFs) or enhanced elemental solubility, but these factors can be influenced by several physical and chemical factors and are not diagnostic of anthropogenic Fe, per se (Baker & Jickells, 2006; Conway et al., 2015).

Recent work has made use of aerosol Fe isotope composition (δ^{56}Fe) as a tracer for natural and anthropogenic Fe (Mead et al., 2013; Kurisu et al., 2016a, 2016b, 2019, 2021, 2024; Conway et al., 2019). Some of these studies have applied a distinct δ^{56}Fe endmember to each source. For example, Conway et al. (2019) utilized δ^{56}Fe as a source tracer in aerosols over the North Atlantic, with an isotopically constrained two-component mixing model, where insoluble natural Fe aerosols exhibit near-crustal δ^{56}Fe (+0.09‰) while more soluble anthropogenic Fe aerosols have very low δ^{56}Fe (−1.6‰). They found crustal Saharan Fe dominated bulk aerosols in the subtropical Atlantic, but up to 100% of soluble Fe was derived from combustion near North America and Europe (Conway et al., 2019). Using aerosols from Japan, Kurisu et al. (2016a, 2016b) showed the δ^{56}Fe of the Asian anthropogenic endmember could be extremely low, but was also particle size-dependent; δ^{56}Fe of large particles was 0.0 to +0.3‰ while the fine particles, which are more likely to be entrained into the upper troposphere and deposited over the ocean, were much lower (particles −3.2 to −0.6‰, water-soluble Fe down to −3.9‰). Based on combustion- and smelting-dominated small aerosol particles releasing soluble Fe as low as −4.7‰, Kurisu et al. (2019) proposed a soluble anthropogenic aerosol δ^{56}Fe endmember of −4.4 ± 0.3‰ for Asian aerosols, lighter than that used for the Atlantic. Using this endmember and two-component mixing, combustion contributes up to 50% of fine and 21% of coarse aerosol Fe over the western North Pacific Ocean, with much lower contributions in the east than west (Kurisu et al., 2021, 2024).

However, one piece of knowledge currently missing for using δ^{56}Fe as a source identification tool is the isotopic signature of wildfire-sourced Fe. Although it has been argued that wildfire Fe is light due to light plant material (Guelke & von Blankenburg, 2007; Guelke-Stelling & von Blanckenburg, 2012; Mead et al., 2013), recent work has identified the importance of pyroconvective soil entrainment during wildfires, where much (potentially two-thirds) of the wildfire-derived Fe may be expected to be sourced from local soils (Hamilton et al., 2022). To date, the only study of δ^{56}Fe from wildfires found the Fe released was heavier than the (combustion-dominated) background, perhaps attributed to soil entrainment (Kurisu and Takashi, 2019). However, direct measurements of the properties of Fe from wildfires are lacking, and as such, use of δ^{56}Fe endmembers to quantify sources remains problematic in areas where wildfire aerosols are prevalent (Hamilton et al., 2020).

Although Zn aerosol concentrations and EFs have been well studied, the use of δ^{66}Zn in open ocean aerosols is a relatively new tracer, and is not nearly as well studied as δ^{56}Fe. To date, only three studies have reported open ocean aerosol δ^{66}Zn and they have all been from the Atlantic Ocean; as such, we lack a global understanding of aerosol δ^{66}Zn systematics. Initial estimates of soluble aerosol δ^{66}Zn from the North Atlantic Ocean showed lithogenic compositions (+0.34 ± 0.14‰; Little et al., 2014), while more recent work from the North and Equatorial Atlantic found bulk and soluble aerosol δ^{66}Zn to vary over a larger range, from −0.12 to +0.41‰ and −0.21 to +0.25‰, respectively, indicative of an anthropogenic contribution (Packman et al., 2022; Zhang et al., 2024), which is thought to be lighter-than-crustal (−1.1 to +0.1‰; Gioia et al., 2008).

Here, we present δ^{56}Fe and δ^{66}Zn from bulk and ultrapure water-leached aerosols and the δ^{56}Fe of size-fractionated bulk aerosols collected during the US GEOTRACES GP15 section, which took place from September–November 2018 (during the low dust season) from Alaska to Tahiti along 152°W (Figure 1a). North Pacific atmospheric circulation has three major features where: (a) westerly winds travel from Asia across the North Pacific, (b) air masses continue across North America, (c) air masses reaching North America are retroflected off the coast and travel back east to Asia (Figure 1a; Parrington et al., 1983; Marsay et al., 2022a, 2022b). Accordingly, here, aerosol deployments are categorized as Asian Outflow (5–11; 52°N to 32°N) or Equatorial Pacific (13–23; 20°N to 20°S) based on 5-day HYSPLIT back trajectory models and general North Pacific atmospheric circulation (Marsay et al., 2022a, 2022b). Deployments 1 and 3 are classified as Margin deployments as they were collected close to the continental margins and are likely dominated by proximal and local sources, as such they are not discussed at length here.

2. Materials and Methods

Aerosol samples were collected as part of the US GEOTRACES GP15 section, with collection, processing, and digestion/leaching techniques previously described (Marsay et al., 2022a, 2022b) or in Supporting Information S1. Aerosol Fe and Zn concentrations and isotopic ratios (δ^{56}Fe and δ^{66}Zn) in digested (bulk or different size-fractions) or ultrapure water leached (soluble) aerosols were determined at USF using a Thermo Neptune MC-ICP-MS following previously published methods (Conway et al., 2019; Sieber et al., 2023a; see Supporting Information S1 for details and uncertainty of ICP-MS measurements).

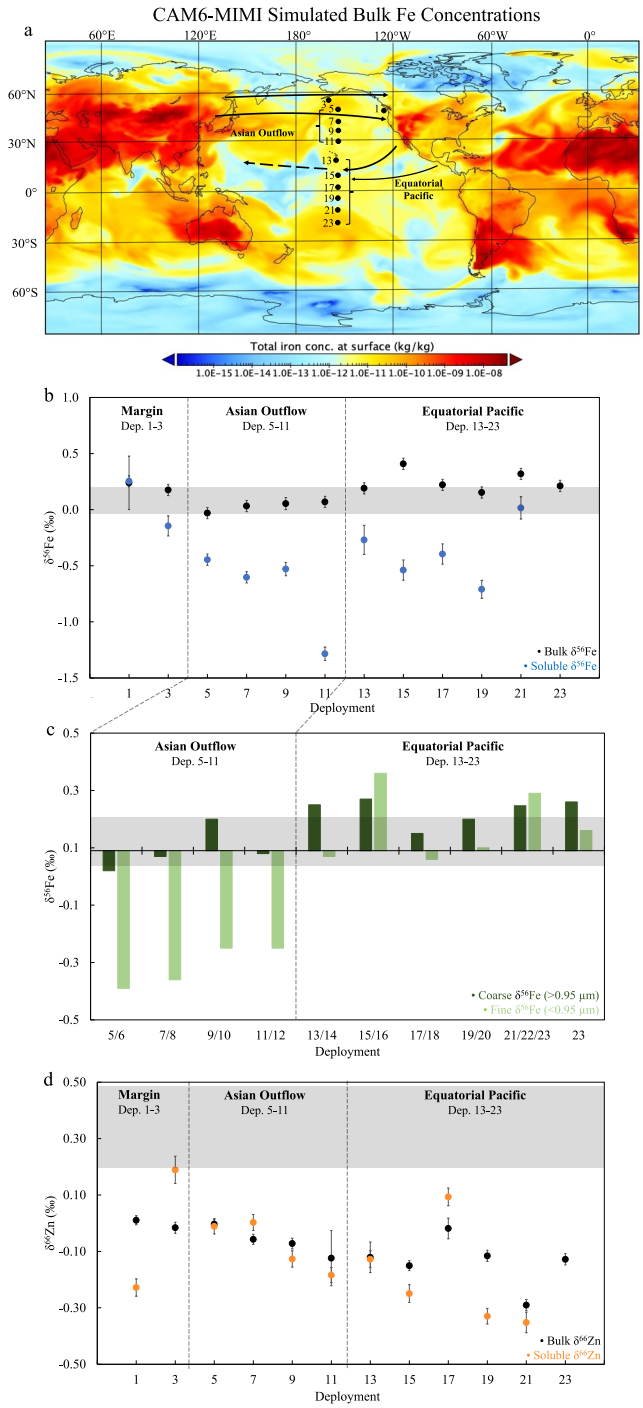

Figure 1. (a) GP15 aerosol deployment map overlaid on CAM6-MIMI bulk aerosol Fe output during GP15 (3 October 2018). (b) GP15 bulk and soluble aerosol δ^{56}Fe, (c) coarse and fine size-fractionated aerosol δ^{56}Fe, and (d) bulk and soluble aerosol δ^{66}Zn. Gray boxes denote the crustal range of δ^{56}Fe (−0.01 to +0.19‰; Gong et al., 2017) and δ^{66}Zn (+0.20 to +0.42‰; Little et al., 2014). Note the size-fractionated deployment latitudes do not overlap exactly with regular deployments and the *x*-axis passes through +0.09‰.

Aerosol Fe data was simulated using the Mechanism of Intermediate complexity for Modeling Iron (MIMI) embedded within the Community Earth System Model's (CESM) atmospheric model: Community Atmosphere Model v6 (CAM6) (Hamilton et al., 2019, 2022). Information regarding errors and uncertainty of the model output can be found in Supporting Information S1. The δ^{56}Fe signature of natural dust is well constrained (+0.09‰), and an anthropogenic signature of −1.60‰ (as proposed by Conway et al. (2019)) was used here as an initial endmember for anthropogenic, shipping, and wildfire δ^{56}Fe. Subsequently, the δ^{56}Fe of anthropogenic, wildfire, and shipping Fe endmembers and CAM6-MIMI concentration output for dust, anthropogenic, and shipping Fe were then all optimized to improve the correlation between model and measured data (see Supporting Information S1).

3. Results

Bulk aerosol Fe during GP15 were elevated within the Asian Outflow study region (37.7–155.1 pmol m^{-3}) compared to the Equatorial Pacific (22.4–65.1 pmol m^{-3}), up to two orders of magnitude lower than the high dust season as sampled on the 2005/2006 CLIVAR P16 cruise (23–2,350 pmol m^{-3}; Buck et al., 2013). GP15 soluble aerosol Fe ranged from 0.3 to 7.1 pmol m^{-3}. Margin deployments bulk Fe was 13.2–36.3 pmol m^{-3} and soluble Fe was 0.9–3.7 pmol m^{-3}. Bulk aerosol Zn was less variable across the entire transect (3.9–17.2 pmol m^{-3}), as was soluble Zn (1.6–8.0 pmol m^{-3}). Compared to nearby data collected during the high dust season (mean 90 pmol m^{-3}; along 160°W, Furutani et al., 2010), bulk GP15 aerosol Zn was an order of magnitude lower.

GP15 Asian Outflow bulk aerosols were identified as crustal (+0.09 ± 0.10‰), with δ^{56}Fe from −0.03‰ to +0.07‰ (Figure 1). By contrast, GP15 Equatorial Pacific bulk aerosols ranged from +0.15‰ to +0.41‰ (Figure 1). Similarly, the coarse size fraction (>0.95 μm) of Asian Outflow aerosols was also crustal (+0.02 to +0.20‰), while the coarse fraction in Equatorial Pacific aerosols were slightly elevated (+0.15 to +0.27‰). Lastly, the fine fraction aerosols (<0.95 μm) were light in the Asian Outflow region (−0.39 to −0.25‰), while Equatorial Pacific aerosols showed slightly higher δ^{56}Fe values in comparison (fine fraction: +0.06 to +0.36‰). Soluble δ^{56}Fe for the Asian Outflow and Equatorial Pacific were both light, ranging from −1.28 to −0.45‰ and −0.71 to +0.02‰, respectively. Size-fractionated samples for Margin deployments are not reported as concentrations were below detection for each filter stage.

Bulk aerosol δ^{66}Zn were consistently lower than crustal (+0.31 ± 0.11‰) within the Asian Outflow and Equatorial Pacific, ranging from −0.12 to 0.00‰ and −0.29 to −0.02‰, respectively (overall mean: −0.12 ± 0.08‰). Similarly, soluble aerosol δ^{66}Zn were also low across the section (overall mean: −0.17 ± 0.14‰), with Asian Outflow soluble Zn aerosols ranging from −0.18 to 0.00‰ and Equatorial Pacific aerosols between −0.35‰ and +0.09‰. Bulk δ^{66}Zn for margin deployments was −0.02‰ to +0.01‰ and soluble δ^{66}Zn was −0.23‰ to +0.19‰.

4. Discussion

First, we discuss sources of aerosol Fe and Zn to the Asian Outflow and Equatorial Pacific deployments, based on δ^{56}Fe and δ^{66}Zn of bulk, soluble, and size-fractionated (only δ^{56}Fe) aerosols of the two regions as well as va-

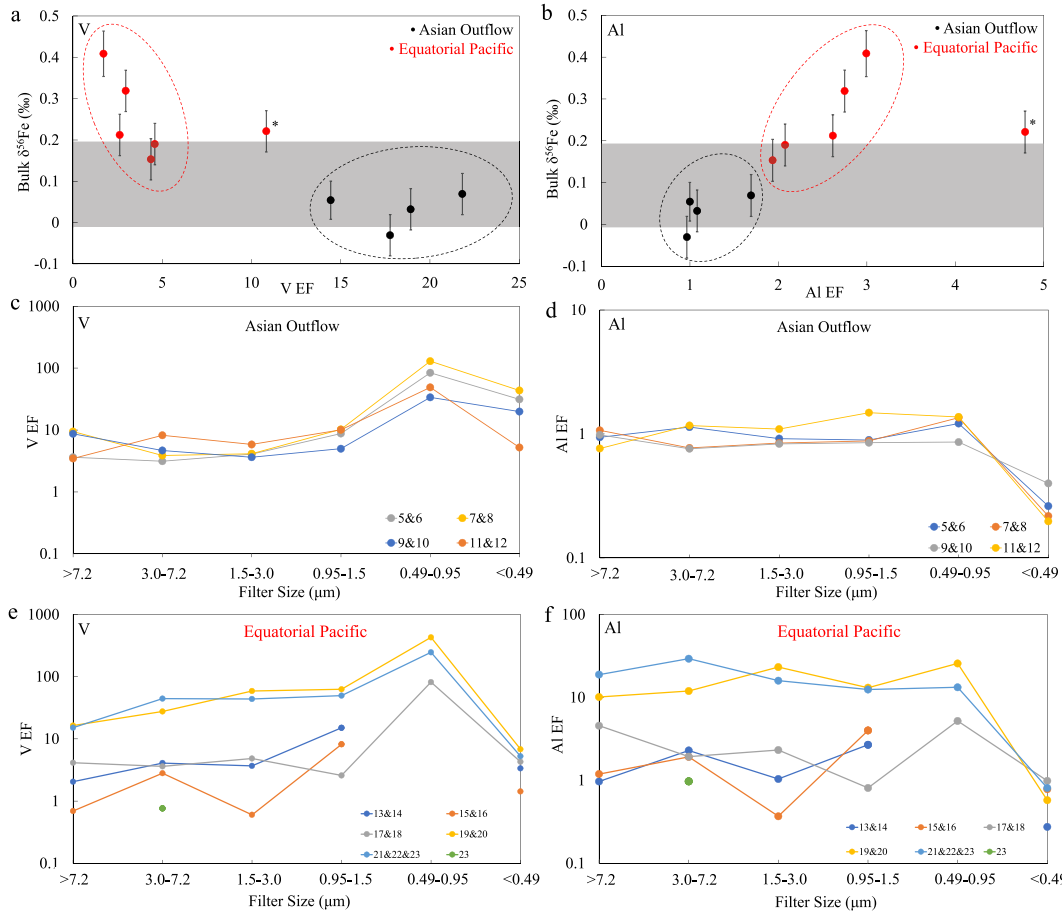

Figure 2. GP15 bulk aerosol δ^{56}Fe compared to V (a) and Al (b) EFs. Gray boxes denote the crustal range of δ^{56}Fe (−0.01 to +0.19‰; Gong et al., 2017), and bulk enrichment factors are from Marsay et al. (2022a, 2022b). Size-fractionated Asian Outflow and Equatorial Pacific V (c), (e) and Al (d), (f) EFs. Note the starred datum not included in fields in a and b is also characterized by elevated V, Cd, Pb EF (Marsay et al., 2022a, 2022b and Figure S1 in Supporting Information S1) suggesting it is influenced by a different mix of sources.

nadium (V; an anthropogenic aerosol tracer) and aluminum (Al; a lithogenic tracer) EFs (from Marsay et al., 2022a, 2022b). GP15 EFs were calculated relative to the Ti content of the sample and Upper Continental Crust (UCC) (taken from Marsay et al., 2022a, 2022b; Equation S3 in Supporting Information S1). Second, we use measured bulk Fe concentrations and δ^{56}Fe with model output to better constrain CAM6-MIMI Fe sources and aerosol δ^{56}Fe endmembers for the North Pacific Ocean (Hamilton et al., 2019, 2022).

4.1. GP15 Bulk Aerosol Fe Sources

Asian Outflow deployments exhibit higher Fe concentrations than Equatorial Pacific deployments. Aerosol Fe traveling from northern Asia to North America is thought to consist of loess from the Chinese Plateau and Gobi/Taklamakan desert dust mixed with anthropogenic aerosols produced around industrial hubs as a result of the transport of dust from Asia (Huang et al., 2010). GP15 bulk and size-fractionated δ^{56}Fe signatures as well as V and Al EFs indicate the source of Fe to Asian Outflow deployments is Asian dust comprised of both crustal and anthropogenic components (Figures 1 and 2). While bulk and coarse aerosol δ^{56}Fe, and Al EFs are all indicative of the presence of lithogenic Fe, fine aerosol δ^{56}Fe was lower indicating the presence of anthropogenic Fe (Figures 1 and 2). Anthropogenic material dominating the fine aerosols is also supported by elevated V EF in the fine fraction (Figure 2). A similar dichotomy between coarse and fine δ^{56}Fe (and anthropogenic contributions) was reported for North Pacific aerosols by Kurisu et al. (2021, 2024).

Based on North Pacific atmospheric circulation, Asian dust retroflects along the coast of California, so Equatorial Pacific deployments are also influenced by some amount of Asian dust. However, bulk, coarse, and fine aerosols are all crustal or slightly heavier, indicating a different and/or additional source supplying elevated δ^{56}Fe compared to the Asian Outflow deployments (Figures 1 and 2). This finding is consistent with Kurisu et al. (2021) and Labatut et al. (2014), who saw δ^{56}Fe values up to +0.42‰ in North Pacific aerosols, observations they were unable to fully explain. Recently, however, Hamilton et al. (2022) calculated up to two-thirds of Fe produced during wildfires is composed of soil-derived Fe (i.e., one-third is likely to be plant-derived Fe in fire plumes). While the range of δ^{56}Fe measured in global soils ranges from −0.5‰ to +0.95‰, Californian soils are in the upper end (+0.20‰ to +0.95‰, Johnson et al., 2020 and references therein). Consequently, elevated δ^{56}Fe in the Equatorial Pacific bulk, coarse, and fine aerosol samples are consistent with wildfire aerosols being influenced by isotopically heavy soil-derived Fe (Figures 1 and 2).

The 2018 Californian wildfire season was one of the largest and most destructive in recent Californian history (~2 million acres burned), with infamous fires such as Camp Fire and Woolsey Fire occurring during GP15 (CAL-FIRE, 2018). Further evidence for a wildfire soil source to GP15 Equatorial Pacific aerosols comes from Al EFs, which are elevated above crustal values—and correlate with bulk aerosol δ^{56}Fe—which can be attributed to the addition of soil trace metals during wildfires (Figure 2). Indeed, Schlosser et al. (2017) showed elements such as Fe and Al to be elevated in Western US wildfire events, which they attributed to soil entrainment, and most recently, Perron et al. (2022) showed a near two-fold increase in Fe and Al aerosol loading during wildfire events in Western Australia. This would provide an alternate explanation to Marsay et al. (2022a, 2022b), who attributed the increase of Al EFs in the Equatorial Pacific to a winnowing effect of coarse mineral dust; however, loss of coarse lithogenic particles would not be expected to lead to an increase in δ^{56}Fe in the bulk phase, and especially not in the small particles as observed here.

Although the bulk and size-fractionated aerosol δ^{56}Fe data from Equatorial Pacific deployments are indicative of the presence of crustal material and wildfire Fe, V EFs are much lower in these aerosols than in those from the Asian Outflow, and correlation between increasing V EFs and decreasing bulk aerosol δ^{56}Fe indicates the presence of some anthropogenic material in these aerosols (Figure 2). Thus, while bulk and size-fractionated δ^{56}Fe and Al EFs suggest the main sources of Fe to the Equatorial Pacific aerosols are crustal material and Californian wildfires, elevated V EFs in the fine fraction also point to anthropogenic Fe either carried with Asian dust or further entrained from industrial areas along North America during transport.

4.2. GP15 Soluble Aerosol Fe Sources

While there is a large disparity between the sources supplying Fe to Asian Outflow and Equatorial Pacific GP15 deployments, soluble Fe aerosols are light throughout the transect (as light as −1.28‰), indicative of more-soluble combustion Fe. There is no obvious difference in soluble δ^{56}Fe between the two regions despite Asian Outflow deployments containing anthropogenic Fe from industrial processes and combustion, and anthropogenic Fe in Equatorial deployments likely originating from a mixture of Californian and Asian industrial sources (and perhaps plant material). Overall, the clear importance of anthropogenic Fe in setting the δ^{56}Fe of Asian Outflow deployment fine particles and to soluble phase aerosol Fe across the GP15 section demonstrate the importance of anthropogenic processes as a source of Fe to oligotrophic North Pacific surface waters which may influence primary productivity to different degrees depending on surface regime (König et al., 2022).

Since there are two prominent Fe sources supplying soluble Fe to the Asian Outflow deployments (dust and anthropogenic Fe), a two-component mixing model (Equation 4) can be utilized to calculate the relative proportions of each source. Using an anthropogenic endmember of −1.6‰ as per Conway et al. (2019), GP15 soluble aerosol Fe within the Asian Outflow contains 32%–81% anthropogenic Fe and 19%–68% dust Fe (Table S1 in Supporting Information S1), indicating the more-soluble anthropogenic Fe comprises a notable proportion of the soluble aerosol phase. If the lighter anthropogenic endmember of −4.3‰ from Kurisu et al. (2019) is used for soluble anthropogenic Fe, this reduces to 12%–31% anthropogenic. Notably, a two-component model cannot be used to calculate the proportion of sources to the Equatorial Pacific deployments as there are likely at least three sources here.

4.3. GP15 Zn Aerosol Sources

Asian Outflow deployments have a mean bulk aerosol δ^{66}Zn of −0.06 ± 0.08‰ and soluble aerosol δ^{66}Zn of −0.05 ± 0.14‰ (±1SD), notably lighter than lithogenic composition (+0.31 ± 0.11‰; Little et al., 2014). Equatorial Pacific deployments had slightly lower means of −0.15 ± 0.10‰ for bulk and −0.24 ± 0.15‰ soluble aerosols. Bulk and soluble δ^{66}Zn along GP15 are, on average, lighter than reported Atlantic data (bulk: −0.12 to +0.41‰, soluble −0.21 to +0.25‰; Packman et al. (2022); Zhang et al. (2024)). This difference is likely due to the high lithogenic content of Atlantic aerosols influenced by Saharan dust, compared to North Pacific aerosols during the low-dust season which are more strongly influenced by Asian anthropogenic sources; this finding is consistent with that for Cd in GP15 aerosols, where low δ^{114}Cd was indicative of the dominance of anthropogenic Cd along the section (Sieber et al., 2023b).

Indeed, the GP15 aerosol δ^{66}Zn data (and elevated Zn EF; Figure S1 in Supporting Information S1) indicate a strong anthropogenic Zn signal in Asian dust compared to a relatively small natural Zn component within Asian Outflow deployments; however, and unlike for Fe, the Equatorial Pacific deployments generally show elevated Zn EF, lighter δ^{66}Zn, and a larger $\Delta\delta^{66}Zn_{bulk\text{-}soluble}$ than in the north (Figure S1 in Supporting Information S1), indicative of a further isotopically light Zn source to the south. Based on our analysis of Fe sources, possible Zn sources along the coast of western North America might be expected to be wildfire soil or plant material and/or anthropogenic pollution. However, only limited literature data exist to establish a wildfire endmember for δ^{66}Zn. Plants preferentially take up light Zn (−0.56 to −0.26‰), but pyroconvective entrainment of soil Zn would be expected to add a near-crustal isotopic signature (+0.2‰ to +0.5‰; Caldelas & Weiss, 2017; Jouvin et al., 2012; Weiss et al., 2007). Similar to Fe, wildfire-derived Zn is likely a mixture of soil and plant derived Zn, with studies of biomass burning showing evidence of aerosols enriched in Zn, possibly also attributed to soil entrainment (Kurisu and Takashi, 2019; Schlosser et al., 2017). However, given the Zn content of soil is typically much lower than Fe (soil has ∼66-55,000× less Zn than Fe; Bodek et al., 1988; Lindsay, 1972), the different ratio of plant to soil Zn (plants only have ∼2–6 times less Zn than Fe; Timperley et al., 1973) would be expected to lead to a wildfire endmember δ^{66}Zn that is more strongly dominated by plants and thus isotopically lighter than lithogenic material.

It is also possible North American anthropogenic Zn could be a source of light Zn to southern GP15 aerosols, but the decrease in bulk and soluble δ^{66}Zn also occurs in tandem with increasing EFs of the apparent wildfire soil tracer, Al, and lower EFs of the anthropogenic tracer, V, as well as correlating with Ni EFs (Figure S1 in Supporting Information S1). These relationships further support a wildfire source of light Zn. We note Perron et al. (2022) showed biomass burning also entrained V and Pb in Western Australia, which they concluded came from contaminated soil. As such, it is also possible light Zn comes from the entrainment of anthropogenically contaminated soils during wildfires, in addition to potential additional anthropogenic sources of Zn from North America. Further work is needed to deconvolute these potential sources.

4.4. CAM6-MIMI—GP15 Comparison

In the Atlantic, aerosol δ^{56}Fe data has previously been used to help optimize aerosol sources using CAM4-MIMI (Conway et al., 2019). Similarly, here, we compared bulk aerosol measurements from GP15 with simulated bulk aerosol Fe data during the low-dust season of 2018 from the newer CAM6-MIMI model to tune model output and provide guidance for future development. The model subdivides bulk Fe concentrations into natural dust, anthropogenic, and wildfire components. Daily model Fe concentrations, correlated to deployment dates, were compared with GP15 concentrations. During this low-dust season, modeled bulk Fe concentrations were up to an order of magnitude larger than measured GP15 concentrations (Figure 3a). We improved this fit by making reasonable adjustments to the magnitude of dust, anthropogenic (land and shipping), and wildfire Fe based on a sum of squares analysis.

An optimized fit was found by reducing dust, anthropogenic, and shipping model Fe emissions to 70%, 25%, and 25% of base values respectively (wildfire was not changed; Figure 3a). Optimization reduced the sum of squares from 149,000 to 23 (Table S2 in Supporting Information S1). Such optimization of the dust emissions is within modeled uncertainties for daily dust concentrations due to the episodic nature of dust events (e.g., Hamilton et al., 2020; Smith et al., 2017). Modeled anthropogenic emissions, however, are consistent with respect to time (lower variability and thus lower uncertainties), and so our optimized fit suggests the base scenario of the model over-estimates anthropogenic Asian Fe sources, transport efficiency, or some combination of both (see

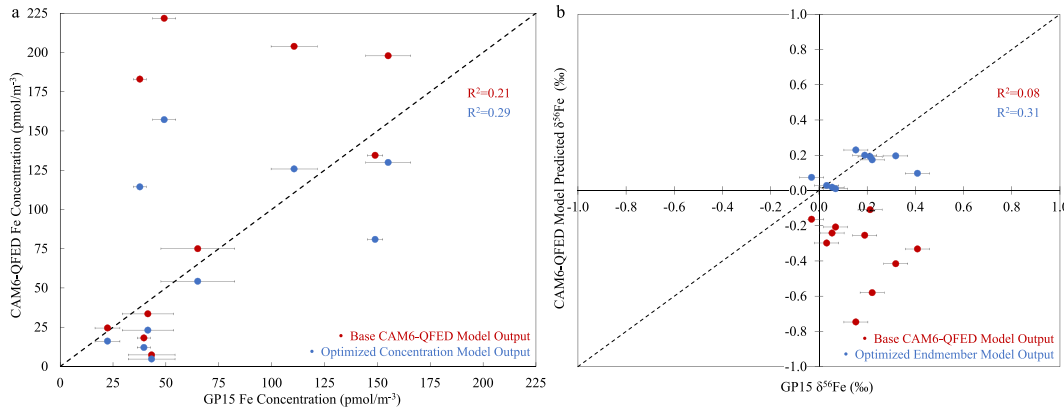

Figure 3. Comparison of base CAM6-MIMI simulated bulk aerosol Fe concentrations (a) and δ^{56}Fe (b) compared to GP15 observations (red points). Optimized CAM6-MIMI simulation (blue points). Optimization, endmembers, and errors described further in Supporting Information S1.

Supporting Information S1) to the western North Pacific region during the low dust season (Rathod et al., 2024). The updated and optimized concentrations of dust, anthropogenic, and shipping Fe calculated by comparing CAM6-MIMI with GP15 were subsequently used to optimize the wildfire and shipping δ^{56}Fe endmembers.

Subsequently, concentration-optimized model sources were assigned δ^{56}Fe endmembers to calculate model-weighted bulk δ^{56}Fe values to compare with GP15 bulk δ^{56}Fe (Figure 3b; Supporting Information S1). Initial endmember choices were from Conway et al. (2019): dust: +0.10‰; wildfire: −1.60‰; anthropogenic: −1.60‰; shipping: −1.60‰. The comparison of model and GP15 bulk δ^{56}Fe showed a large disparity, with the model predicting much lighter compositions than observations (Figure 3b). We explored what might be driving this offset by varying δ^{56}Fe endmembers (see Supporting Information S1), with the fit between CAM6-MIMI and GP15 data assessed using SoSs (Table S3 in Supporting Information S1). The optimal endmembers were +0.10‰ (dust), +0.80‰ (wildfire), −1.6‰ (anthropogenic), and +0.5‰ (shipping), reducing the SoSs from 17 to 0.14 (Table S3 in Supporting Information S1; Figure 3b).

How do these findings compare to observations? The crustal endmember is well-constrained and has not been changed. A constrained wildfire endmember has remained elusive due to lack of data and the dichotomy of wildfires likely being a mixture of (heavy) soil Fe and (light?) biomass Fe. While an optimal endmember choice of +0.8‰ is consistent with a dominant Californian soil contribution to wildfire Fe (+0.2 to +1.0‰; Johnson et al., 2020), we note using +0.4‰ (reflecting a contribution of light plant material) only changes the SoS from 0.14 to 0.23 (Figure 3b; Table S3 in Supporting Information S1), suggesting there is some flexibility, and the dynamics of different fires can be represented. This supports the explanation of the contribution of a heavy wildfire endmember to the Equatorial Pacific deployments in this study. The shipping endmember found here is consistent with the coarse fraction of anthropogenic combustion and of isotopically heavy fuel oil products which may be added to open ocean waters by container vessels (+0.3‰, Kurisu et al., 2016a; +0.5‰, Mead et al., 2013). There was a negligible effect on the overall fit by varying between these values (Table S3 in Supporting Information S1). We also note the effect of varying each source depends on the deployment location. Changing the shipping endmember predominantly influences the Asian Outflow deployments (a prominent shipping corridor) while altering the wildfire endmember drastically affects the Equatorial Pacific deployments (downwind of active fire regions). While this gives a first estimate of these endmembers, additional work is needed to constrain shipping and wildfire δ^{56}Fe aerosol endmembers in other regions of the world.

Lastly, a comment on the anthropogenic endmember. Kurisu et al. (2019) proposed −4.3‰ for soluble anthropogenic aerosols, lighter than our optimized endmember. However, applying −4.3‰ to model output resulted in a much worse model-data fit (Table S3 and Figure S2 in Supporting Information S1), suggesting this endmember is too light for the bulk phase. However, the two findings are not inconsistent, since Kurisu et al.'s endmember was based only on the soluble phase of the most highly fractionated small anthropogenic particles (see Supporting Information S1), and as such is likely not appropriate for use in calculations of the anthropogenic contribution to the bulk aerosol particles, which contain a range of particle sizes, including larger particles with

heavier isotope compositions. As for the other sources, future work is needed to continue to refine the most-relevant anthropogenic endmembers for different phases of marine aerosols.

5. Conclusions

Asian Outflow and Equatorial GP15 aerosol deployments display contrasts between bulk and size-fractionated δ^{56}Fe as well as V, Al and Zn EF due to a different relative contribution of sources. While northern bulk δ^{56}Fe are crustal, isotopically light fine particles and elevated V EFs both indicate the presence of anthropogenic material. By contrast, isotopically heavy bulk aerosol Fe in the south, correlated with elevated Al EFs, indicates wildfires from North America are an additional source of Fe to Equatorial Pacific aerosols. We attribute this signal to pyroconvective entrainment of soil into wildfire smoke plumes along the coast of California during the burning season. The importance of soil for raising the δ^{56}Fe of bulk aerosol is consistent with previous work (Kurisu and Takashi, 2019) and corroborated by comparing GP15 data with daily output from a global iron aerosol model (CAM6-MIMI; Hamilton et al., 2019, Hamilton et al., 2022), which also shows anthropogenic and dust Fe sources are overestimated in the model. When considering the soluble supply of Fe to the North Pacific, however, similar light δ^{56}Fe in both Asian Outflow and Equatorial Pacific samples suggest anthropogenic Fe is a significant component of soluble Fe throughout the GP15 section. Unlike aerosol Fe, both bulk and soluble Zn aerosols from GP15 are dominated by light anthropogenic Zn, with a possible wildfire component in the south, and show a relatively homogenous composition (bulk: $-0.12 \pm 0.08‰$ and soluble: $-0.17 \pm 0.14‰$) along the transect. The similarity between the mean isotopic composition of bulk and soluble GP15 aerosols, and the small standard deviations of each provides a robust estimate of the isotopic signature of atmospheric Zn to the North Pacific, at least during the low-dust season.

Data Availability Statement

Bulk, soluble, and size-fractionated aerosol Fe and Zn data have been accepted by the Biological and Chemical Oceanography Data Management Office and are available for free via Conway et al. (2024a, 2024b). CAM6-MIMI bulk aerosol Fe data can be found via Hamilton et al. (2022).

Acknowledgments
We thank those aboard the GP15 cruise, and Ethan Goddard for technical assistance. This work was supported by NSF awards (OCE-1737136 TMC, OCE-1736896 SGJ, OCE-1756103 CSB, OCE-1756104 WML), and USF Paul Getting and Kent Fanning Fellowships ZB. DSH acknowledges support from NASA (Grant 80NSSC24K0446), and from Cheyenne (https://doi.org/10.5065/D6RX99HX) by NCAR's Computational and Information Systems Laboratory, sponsored by NSF. The International GEOTRACES programme is possible thanks to support from NSF Grant OCE-2140395 to SCOR.

References

Baker, A. R., & Jickells, T. D. (2006). Mineral particle size as a control on aerosol iron solubility. *Geophysical Research Letters*, *33*(17), L17608. https://doi.org/10.1029/2006gl026557

Bodek, I., Lyman, W. J., Reehl, W. F., & Rosenblatt, D. H. (Eds.) (1988). *Environmental inorganic chemistry: Properties, processes, and estimation methods* (Vol. 10). Pergamon press.

Buck, C. S., Landing, W. M., & Resing, J. (2013). Pacific Ocean aerosols: Deposition and solubility of iron, aluminum, and other trace elements. *Marine Chemistry*, *157*, 117–130. https://doi.org/10.1016/j.marchem.2013.09.005

Caldelas, C., & Weiss, D. J. (2017). Zinc homeostasis and isotopic fractionation in plants: A review. *Plant and Soil*, *411*(1–2), 17–46. https://doi.org/10.1007/s11104-016-3146-0

CALFIRE. (2018). *2018 incident archive*. California Department of Fire and Forest Protection. Retrieved from https://www.fire.ca.gov/incidents/2018

Conway, T. M., Buck, C. S., John, S. G., Landing, W. M., & Marsay, C. (2024a). Concentrations and stable isotopes of total and deionized water-soluble Fe, Zn, and Cd bulk aerosols and Fe concentrations and stable isotopes of coarse and fine aerosols from Leg 1 of the US GEOTRACES PMT cruise (GP15, RR1814) from Sept to Oct 2018 (Version 1) [Dataset]. *Biological and Chemical Oceanography Data Management Office (BCO-DMO)*. https://doi.org/10.26008/1912/BCO-DMO.937120.1

Conway, T. M., Buck, C. S., John, S. G., Landing, W. M., & Marsay, C. (2024b). Concentrations and stable isotopes of total and deionized water-soluble Fe, Zn, and Cd bulk aerosols and Fe concentrations and stable isotopes of coarse and fine aerosols from Leg 2 of the US GEOTRACES PMT cruise (GP15, RR1814) from Oct to Nov 2018 (Version 1) [Dataset]. *Biological and Chemical Oceanography Data Management Office (BCO-DMO)*. https://doi.org/10.26008/1912/BCO-DMO.937148.1

Conway, T. M., Hamilton, D. S., Shelley, R. U., Aguilar-Islas, A. M., Landing, W. M., Mahowald, N. M., & John, S. G. (2019). Tracing and constraining anthropogenic aerosol iron fluxes to the North Atlantic Ocean using iron isotopes. *Nature Communications*, *10*(1), 2628. https://doi.org/10.1038/s41467-019-10457-w

Conway, T. M., Middag, R., & Schlitzer, R. (2024). GEOTRACES: Ironing out the details of the oceanic iron sources? *Oceanography*, *27*(2), 35–45. https://doi.org/10.5670/oceanog.2024.416

Conway, T. M., Wolff, E. W., Röthlisberger, R., Mulvaney, R., & Elderfield, H. E. (2015). Constraints on soluble aerosol iron flux to the southern ocean at the last glacial maximum. *Nature Communications*, *6*(1), 7850. https://doi.org/10.1038/ncomms8850

Furutani, H., Meguro, A., Iguchi, H., & Uematsu, M. (2010). Geographical distribution and sources of phosphorus in atmospheric aerosol over the North Pacific Ocean. *Geophysical Research Letters*, *37*(3), L03805. https://doi.org/10.1029/2009gl041367

Gioia, S., Weiss, D., Coles, B., Arnold, T., & Babinski, M. (2008). Accurate and precise zinc isotope ratio measurements in urban aerosols. *Analytical chemistry*, *80*(24), 9776–9780. https://doi.org/10.1021/ac8019587

Gong, Y., Xia, Y., Huang, F., & Yu, H. (2017). Average iron isotopic compositions of the upper continental crust: Constrained by loess from the Chinese Loess Plateau. *Acta Geochimica*, *36*(2), 125–131. https://doi.org/10.1007/s11631-016-0131-5

Guelke, M., & Von Blanckenburg, F. (2007). Fractionation of stable iron isotopes in higher plants. *Environmental Science & Technology*, *41*(6), 1896–1901. https://doi.org/10.1021/es062288j

Guelke-Stelling, M., & von Blanckenburg, F. (2012). Fe isotope fractionation caused by translocation of iron during growth of bean and oat as models of strategy I and II plants. *Plant and Soil*, *352*(1–2), 217–231. https://doi.org/10.1007/s11104-011-0990-9

Hamilton, D. S., Perron, M. M., Bond, T. C., Bowie, A. R., Buchholz, R. R., Guieu, C., et al. (2022). Earth, wind, fire, and pollution: Aerosol nutrient sources and impacts on ocean biogeochemistry. *Annual Review of Marine Science*, *14*(1), 303–330. https://doi.org/10.1146/annurev-marine-031921-013612

Hamilton, D. S., Scanza, R. A., Feng, Y., Guinness, J., Kok, J. F., Li, L., et al. (2019). Improved methodologies for Earth system modelling of atmospheric soluble iron and observation comparisons using the Mechanism of Intermediate complexity for Modelling Iron (MIMI v1. 0). *Geoscientific Model Development*, *12*(9), 3835–3862. https://doi.org/10.5194/gmd-12-3835-2019

Hamilton, D. S., Scanza, R. A., Rathod, S. D., Bond, T. C., Kok, J. F., Li, L., et al. (2020). Recent (1980 to 2015) trends and variability in daily-to-interannual soluble iron deposition from dust, fire, and anthropogenic sources. *Geophysical Research Letters*, *47*(17), e2020GL089688. https://doi.org/10.1029/2020gl089688

Huang, K., Zhuang, G., Li, J., Wang, Q., Sun, Y., Lin, Y., & Fu, J. S. (2010). Mixing of Asian dust with pollution aerosol and the transformation of aerosol components during the dust storm over China in spring 2007. *Journal of Geophysical Research*, *115*(D7), D00K13. https://doi.org/10.1029/2009jd013145

Johnson, C., Beard, B., & Weyer, S. (2020). *Iron geochemistry: An isotopic perspective* (p. 360). Springer.

Jouvin, D., Weiss, D. J., Mason, T. F. M., Bravin, M. N., Louvat, P., Zhao, F., et al. (2012). Stable isotopes of Cu and Zn in higher plants: Evidence for Cu reduction at the root surface and two conceptual models for isotopic fractionation processes. *Environmental Science & Technology*, *46*(5), 2652–2660. https://doi.org/10.1021/es202587m

König, D., Conway, T. M., Hamilton, D. S., & Tagliabue, A. (2022). Surface ocean biogeochemistry regulates the impact of anthropogenic aerosol Fe deposition on the cycling of iron and iron isotopes in the North Pacific. *Geophysical Research Letters*, *49*(13), e2022GL098016. https://doi.org/10.1029/2022gl098016

Kurisu, M., Adachi, K., Sakata, K., & Takahashi, Y. (2019). Stable isotope ratios of combustion iron produced by evaporation in a steel plant. *ACS Earth and Space Chemistry*, *3*(4), 588–598. https://doi.org/10.1021/acsearthspacechem.8b00171

Kurisu, M., Sakata, K., Miyamoto, C., Takaku, Y., Iizuka, T., & Takahashi, Y. (2016). Variation of iron isotope ratios in anthropogenic materials emitted through combustion processes. *Chemistry Letters*, *45*(8), 970–972. https://doi.org/10.1246/cl.160451

Kurisu, M., Sakata, K., Nishioka, J., Obata, H., Conway, T. M., Hunt, H. R., et al. (2024). Source and fate of atmospheric iron supplied to the subarctic North Pacific traced by stable iron isotope ratios. *Geochimica et Cosmochimica Acta*, *378*, 168–185. https://doi.org/10.1016/j.gca.2024.06.009

Kurisu, M., Sakata, K., Uematsu, M., Ito, A., & Takahashi, Y. (2021). Contribution of combustion Fe in marine aerosols over the northwestern Pacific estimated by Fe stable isotope ratios. *Atmospheric Chemistry and Physics*, *21*(20), 16027–16050. https://doi.org/10.5194/acp-21-16027-2021

Kurisu, M., & Takahashi, Y. (2019). Testing iron stable isotope ratios as a signature of biomass burning. *Atmosphere*, *10*(2), 76. https://doi.org/10.3390/atmos10020076

Kurisu, M., Takahashi, Y., Iizuka, T., & Uematsu, M. (2016b). Very low isotope ratio of iron in fine aerosols related to its contribution to the surface ocean. *Journal of Geophysical Research: Atmospheres*, *121*(18), 11–119. https://doi.org/10.1002/2016jd024957

Labatut, M., Lacan, F., Pradoux, C., Chmeleff, J., Radic, A., Murray, J. W., et al. (2014). Iron sources and dissolved-particulate interactions in the seawater of the Western Equatorial Pacific, iron isotope perspectives. *Global Biogeochemical Cycles*, *28*(10), 1044–1065. https://doi.org/10.1002/2014gb004928

Lindsay, W. L. (1972). Zinc in soils and plant nutrition. *Advances in Agronomy*, *24*, 147–186. https://doi.org/10.1016/s0065-2113(08)60635-5

Little, S. H., Vance, D., Walker-Brown, C., & Landing, W. M. (2014). The oceanic mass balance of copper and zinc isotopes, investigated by analysis of their inputs, and outputs to ferromanganese oxide sediments. *Geochimica et Cosmochimica Acta*, *125*, 673–693. https://doi.org/10.1016/j.gca.2013.07.046

Marsay, C. M., Kadko, D., Landing, W. M., & Buck, C. S. (2022a). Bulk aerosol trace element concentrations and deposition fluxes during the US GEOTRACES GP15 Pacific Meridional Transect. *Global Biogeochemical Cycles*, *36*(2), e2021GB007122. https://doi.org/10.1029/2021gb007122

Marsay, C. M., Landing, W. M., Umstead, D., Till, C. P., Freiberger, R., Fitzsimmons, J. N., et al. (2022b). Does sea spray aerosol contribute significantly to aerosol trace element loading? A case study from the us GEOTRACES Pacific Meridional transect (GP15). *Global Biogeochemical Cycles*, *36*(8), e2022GB007416. https://doi.org/10.1029/2022gb007416

Mead, C., Herckes, P., Majestic, B. J., & Anbar, A. D. (2013). Source apportionment of aerosol iron in the marine environment using iron isotope analysis. *Geophysical Research Letters*, *40*(21), 5722–5727. https://doi.org/10.1002/2013gl057713

Moore, C. M., Mills, M. M., Arrigo, K. R., Berman-Frank, I., Bopp, L., Boyd, P. W., et al. (2013). Processes and patterns of oceanic nutrient limitation. *Nature Geoscience*, *6*(9), 701–710. https://doi.org/10.1038/ngeo1765

Morel, F. M. M., Reinfelder, J. R., Roberts, S. B., Chamberlain, C. P., Lee, J. G., & Yee, D. (1994). Zinc and carbon co-limitation of marine phytoplankton. *Nature*, *369*(6483), 740–742. https://doi.org/10.1038/369740a0

Packman, H., Little, S. H., Baker, A. R., Bridgestock, L., Chance, R. J., Coles, B. J., et al. (2022). Tracing natural and anthropogenic sources of aerosols to the Atlantic Ocean using Zn and Cu isotopes. *Chemical Geology*, *610*, 121091. https://doi.org/10.1016/j.chemgeo.2022.121091

Parrington, J. R., Zoller, W. H., & Aras, N. K. (1983). Asian dust: Seasonal transport to the Hawaiian Islands. *Science*, *220*(4593), 195–197. https://doi.org/10.1126/science.220.4593.195

Perron, M. M., Meyerink, S., Corkill, M., Strzelec, M., Proemse, B. C., Gault-Ringold, M., et al. (2022). Trace elements and nutrients in wildfire plumes to the southeast of Australia. *Atmospheric Research*, *270*, 106084. https://doi.org/10.1016/j.atmosres.2022.106084

Rathod, S., Hamilton, D. S., Nino, L., Kreidenweis, S. M., Bian, Q., Mahowald, N. M., et al. (2024). Constraining present-day anthropogenic total iron emissions using model and observations. *Journal of Geophysical Research: Atmospheres*, *129*(17), e2023JD040332. https://doi.org/10.1029/2023jd040332

Schlosser, J. S., Braun, R. A., Bradley, T., Dadashazar, H., MacDonald, A. B., Aldhaif, A. A., et al. (2017). Analysis of aerosol composition data for western United States wildfires between 2005 and 2015: Dust emissions, chloride depletion, and most enhanced aerosol constituents. *Journal of Geophysical Research: Atmospheres*, *122*(16), 8951–8966. https://doi.org/10.1002/2017jd026547

Sieber, M., Lanning, N. T., Bian, X., Yang, S. C., Takano, S., Sohrin, Y., et al. (2023a). The importance of reversible scavenging for the marine Zn cycle evidenced by the distribution of zinc and its isotopes in the Pacific Ocean. *Journal of Geophysical Research: Oceans*, *128*(4), e2022JC019419. https://doi.org/10.1029/2022jc019419

Sieber, M., Lanning, N. T., Bunnell, Z. B., Bian, X., Yang, S. C., Marsay, C. M., et al. (2023b). Biological, physical, and atmospheric controls on the distribution of cadmium and its isotopes in the Pacific Ocean. *Global Biogeochemical Cycles*, *37*(2), e2022GB007441. https://doi.org/10.1029/2022gb007441

Smith, M. B., Mahowald, N. M., Albani, S., Perry, A., Losno, R., Qu, Z., et al. (2017). Sensitivity of the interannual variability of mineral aerosol simulations to meteorological forcing dataset. *Atmospheric Chemistry and Physics*, *17*(5), 3253–3278. https://doi.org/10.5194/acp-17-3253-2017

Tagliabue, A., Bowie, A. R., Boyd, P. W., Buck, K. N., Johnson, K. S., & Saito, M. A. (2017). The integral role of iron in ocean biogeochemistry. *Nature*, *543*(7643), 51–59. https://doi.org/10.1038/nature21058

Tang, W., Llort, J., Weis, J., Perron, M. M., Basart, S., Li, Z., et al. (2021). Widespread phytoplankton blooms triggered by 2019–2020 Australian wildfires. *Nature*, *597*(7876), 370–375. https://doi.org/10.1038/s41586-021-03805-8

Timperley, M. H., Brooks, R. R., & Peterson, P. J. (1973). The distribution of nickel, copper, zinc, and iron in tree leaves. *Journal of Experimental Botany*, *24*(5), 889–895. https://doi.org/10.1093/jxb/24.5.889

Weiss, D. J., Rausch, N., Mason, T. F., Coles, B. J., Wilkinson, J. J., Ukonmaanaho, L., et al. (2007). Atmospheric deposition and isotope biogeochemistry of zinc in ombrotrophic peat. *Geochimica et Cosmochimica Acta*, *71*(14), 3498–3517. https://doi.org/10.1016/j.gca.2007.04.026

Zhang, X., Lemaitre, N., Rickli, J. D., Suhrhoff, T. J., Shelley, R., Benhra, A., et al. (2024). Tracing anthropogenic aerosol trace metal sources in the North Atlantic Ocean using Pb, Zn and Ni isotopes. *Marine Chemistry*, *258*, 104347. https://doi.org/10.1016/j.marchem.2023.104347

References From the Supporting Information

Archer, C., Andersen, M. B., Cloquet, C., Conway, T. M., Dong, S., Ellwood, M., et al. (2017). Inter-calibration of a proposed new primary reference standard AA-ETH Zn for zinc isotopic analysis. *Journal of Analytical Atomic Spectrometry*, *32*(2), 415–419. https://doi.org/10.1039/c6ja00282j

Buck, C. S., Landing, W. M., Resing, J. A., & Lebon, G. T. (2006). Aerosol iron and aluminum solubility in the northwest Pacific Ocean: Results from the 2002 IOC cruise. *Geochemistry, Geophysics, Geosystems*, *7*(4), Q04M07. https://doi.org/10.1029/2005gc000977

Buck, C., Fietz, S., Hamilton, D., Ho, T. Y., Perron, M., & Shelley, R. (2024). GEOTRACES: Fifteen years of progress in marine aerosol research. *Oceanography*, *37*(2), 98–101. https://doi.org/10.5670/oceanog.2024.409

Buck, C. S., Landing, W. M., & Resing, J. A. (2010). Particle size and aerosol iron solubility: A high-resolution analysis of Atlantic aerosols. *Marine Chemistry*, *120*(1–4), 14–24. https://doi.org/10.1016/j.marchem.2008.11.002

Claquin, T., Schulz, M., & Balkanski, Y. J. (1999). Modeling the mineralogy of atmospheric dust sources. *Journal of Geophysical Research*, *104*(D18), 22243–22256.

Conway, T. M., Rosenberg, A. D., Adkins, J. F., & John, S. G. (2013). A new method for precise determination of iron, zinc and cadmium stable isotope ratios in seawater by double-spike mass spectrometry. *Analytica Chimica Acta*, *793*, 44–52. https://doi.org/10.1016/j.aca.2013.07.025

Gonçalves Ageitos, M., Obiso, V., Miller, R. L., Jorba, O., Klose, M., Dawson, M., et al. (2023). Modeling dust mineralogical composition: Sensitivity to soil mineralogy atlases and their expected climate impacts. *Atmospheric Chemistry and Physics*, *23*(15), 8623–8657. https://doi.org/10.5194/acp-23-8623-2023

Gurganus, S. C., Wozniak, A. S., & Hatcher, P. G. (2015). Molecular characteristics of the water-soluble organic matter in size-fractionated aerosols collected over the North Atlantic Ocean. *Marine Chemistry*, *170*, 37–48. https://doi.org/10.1016/j.marchem.2015.01.007

Hunt, H. R., Summers, B. A., Sieber, M., Krisch, S., Al-Hashem, A., Hopwood, M., et al. (2022). Distinguishing the influence of sediments, the Congo River, and water-mass mixing on the distribution of iron and its isotopes in the Southeast Atlantic Ocean. *Marine Chemistry*, *247*, 104181. https://doi.org/10.1016/j.marchem.2022.104181

Ito, A., & Miyakawa, T. (2023). Aerosol iron from metal production as a secondary source of bioaccessible iron. *Environmental Science & Technology*, *57*(10), 4091–4100. https://doi.org/10.1021/acs.est.2c06472

Li, L., Mahowald, N. M., Kok, J. F., Liu, X., Wu, M., Leung, D. M., et al. (2022). Importance of different parameterization changes for the updated dust cycle modeling in the Community Atmosphere Model (version 6.1). *Geoscientific Model Development*, *15*(22), 8181–8219. https://doi.org/10.5194/gmd-15-8181-2022

Liu, X., Ma, P. L., Wang, H., Tilmes, S., Singh, B., Easter, R. C., et al. (2016). Description and evaluation of a new four-mode version of the modal aerosol Module (MAM4) within version 5.3 of the community Atmosphere model. *Geoscientific Model Development*, *9*(2), 505–522. https://doi.org/10.5194/gmd-9-505-2016

Morton, P. L., Landing, W. M., Hsu, S. C., Milne, A., Aguilar-Islas, A. M., Baker, A. R., et al. (2013). Methods for the sampling and analysis of marine aerosols: Results from the 2008 GEOTRACES aerosol intercalibration experiment. *Limnology and Oceanography: Methods*, *11*(2), 62–78. https://doi.org/10.4319/lom.2013.11.62

Ochoa Gonzalez, R., & Weiss, D. (2015). Zinc isotope variability in three coal-fired power plants: A predictive model for determining isotopic fractionation during combustion. *Environmental Science & Technology*, *49*(20), 12560–12567. https://doi.org/10.1021/acs.est.5b02402

Rathod, S. D., Hamilton, D. S., Mahowald, N. M., Klimont, Z., Corbett, J. J., & Bond, T. C. (2020). A mineralogy-based anthropogenic combustion-iron emission inventory. *Journal of Geophysical Research: Atmospheres*, *125*(17), e2019JD032114. https://doi.org/10.1029/2019jd032114

Scanza, R. A., Hamilton, D. S., Perez Garcia-Pando, C., Buck, C., Baker, A., & Mahowald, N. M. (2018). Atmospheric processing of iron in mineral and combustion aerosols: Development of an intermediate-complexity mechanism suitable for Earth system models. *Atmospheric Chemistry and Physics*, *18*(19), 14175–14196. https://doi.org/10.5194/acp-18-14175-2018

Scanza, R. A., Mahowald, N., Ghan, S., Zender, C. S., Kok, J. F., Liu, X., et al. (2015). Modeling dust as component minerals in the community Atmosphere model: Development of framework and impact on radiative forcing. *Atmospheric Chemistry and Physics*, *15*(1), 537–561. https://doi.org/10.5194/acp-15-537-2015

Schutgens, N., Tsyro, S., Gryspeerdt, E., Goto, D., Weigum, N., Schulz, M., & Stier, P. (2017). On the spatio-temporal representativeness of observations. *Atmospheric Chemistry and Physics*, *17*(16), 9761–9780. https://doi.org/10.5194/acp-17-9761-2017

Sieber, M., Conway, T. M., de Souza, G. F., Hassler, C. S., Ellwood, M. J., & Vance, D. (2021). Isotopic fingerprinting of biogeochemical processes and iron sources in the iron-limited surface Southern Ocean. *Earth and Planetary Science Letters*, *567*, 116967. https://doi.org/10.1016/j.epsl.2021.116967

Sieber, M., Conway, T. M., de Souza, G. F., Obata, H., Takano, S., Sohrin, Y., & Vance, D. (2019). Physical and biogeochemical controls on the distribution of dissolved cadmium and its isotopes in the Southwest Pacific Ocean. *Chemical Geology*, *511*, 494–509. https://doi.org/10.1016/j.chemgeo.2018.07.021

10.1029/2024GL113877

Erratum

The originally published version of this article contained an error in the heading for Section 4.3. "GP14 Zn Aerosol Sources" has been corrected to "GP15 Zn Aerosol Sources." This may be considered the authoritative version of record.